Influence of deviations from ideal stoichiometry on the anisotropy parameters of magnetite $Fe_{3(1-\delta)}O_4$

Z. Kąkol* and J. M. Honig
Department of Chemistry, Purdue University, West Lafayette, Indiana 47907
(Received 3 March 1989)

Magnetization measurements are reported for $Fe_{3(1-\delta)}O_4$ in the range $0 \leq \delta < 0.010$. Anisotropy parameters consistent with these measurements were determined as a function of δ and of temperature T both above and below the Verwey transition temperature. Analysis of the results indicates that the magnetic properties of magnetite are not solely determined by single-ion anisotropies. None of the anisotropy parameters exhibited shifts or slope discontinuities at the critical value δ_c, where the Verwey transition undergoes a change in thermodynamic order; this is taken to indicate that the transition is not driven primarily by magnetic interactions.

I. INTRODUCTORY COMMENTS

The physical properties of magnetite have been investigated numerous times ever since the pioneering studies by Verwey and co-workers,[1] who reported a phase transformation near 120 K, termed the Verwey transition, which is still not understood. Recent intensive investigations[2–4] on carefully prepared specimens of $Fe_{3(1-\delta)}O_4$ have revealed the following features: The transition temperature T_v is greatly reduced with increasing δ; also, in the range $-0.005 < \delta < \delta_c = 0.0039$ the transition is of first order, whereas for $\delta_c < \delta \lesssim 0.012$ it is of second (or higher) order. These features were established primarily through heat capacity, resistivity, and Seebeck coefficient measurements.

An enormous literature had also built up on the magnetic properties, before it was generally recognized that these phenomena depend very sensitively on the oxygen-metal stoichiometry of magnetite. It therefore seemed appropriate to launch another investigation specifically intended to elucidate the dependence of the magnetocrystalline anisotropy of $Fe_{3(1-\delta)}O_4$ on the stoichiometry parameter δ.

The Verwey transition is accompanied by a small change in structure: above and below T_v magnetite is in the cubic inverse spinel[5] $(Fe^{3+})[Fe^{2+},Fe^{3+}]O_4$ and in a monoclinic configuration[6] respectively. The slight concomitant distortion engenders significant changes in the magnetocrystalline anisotropy: Above T_v magnetite has its hard, intermediate, and easy axes along the cubic $\langle 001 \rangle$, $\langle 110 \rangle$, and $\langle 111 \rangle$ directions respectively.[7] Below T_v these axes coincide with the monoclinic a (cubic $[1\bar{1}0]$) b (cubic [110]), and c (cubic [001]) directions. The monoclinic c axis is actually tilted $\sim 0.20(3)°$ away from the vertical toward the $-a$ direction due to a rhombohedral elongation along the $[\bar{1}11]$, or $[\bar{1}1\bar{1}]$ axes,[11] which results in twinning of the crystals.[8–11] The monoclinic c axis may thus be oriented along any of the possible cube edges; hence, it is necessary to apply an external magnetic[11] field H_{ex} to render one of them the preferred easy axis of magnetization.

It is also necessary to take congnizance of axis switching: When H_{ex} is rotated the easy axis of magnetization readily switches from one cube edge to another. This fact limits the fields that can be applied at any given temperature and for any particular specimen, and thus restricts the range of measurements of anisotropy parameters. The reader is referred to several key surveys[10,12,13] for further discussions of the axis-switching process.

II. EXPERIMENTAL TECHNIQUES

Single crystals were prepared from starting materials of 99.999% purity in a skull melter,[14] then oriented, cut, and reannealed under a buffered CO-CO_2 atmosphere,[15] using an oxygen transfer cell[16] to monitor the oxygen fugacity. The samples were quenched and trimmed so as to obtain $Fe_{3(1-\delta)}O_4$ specimens with a uniform composition; these crystals were then ground into spherical shapes. $M(H_{ex})$ magnetization curves were measured on a vibrating sample magnetometer, with H_{ex} aligned along the principal directions of the low- and high-temperature phases.

Typical magnetization curves for samples with $\delta = 0$ (first-order transition) and $\delta = 0.0045$ (second-order transition) at room temperature are shown in Fig. 1(a) and 1(b) as plots of M versus $H_{eff} = H_{ex} - H_D$, where H_D is the demagnetization field. The latter was determined from the initial slopes of the M versus H_{ex} plots; the calculated demagnetization factor N was in the range $4.05 \leq N \leq 4.25$, quite close to the theoretical value $N = 4\pi/3 = 4.19$ for perfect spheres.

Below T_v measurements were performed in $(1\bar{1}0)$ and (111) planes after the samples had been cooled in a magnetic field at an angle of $\sim 35°$ from [001] (i.e., along the [112] direction). As was established by Hamilton,[5] this procedure defines a unique easy axis along a specific [001] direction and also removes the a-b type of twinning; however, the a-a type of twinning is not eliminated in this procedure since orthorhombic elongation along either the $[\bar{1}11]$ or $[\bar{1}1\bar{1}]$ directions is still possible. Magnetization curves in this T range were taken along [001], [110], and

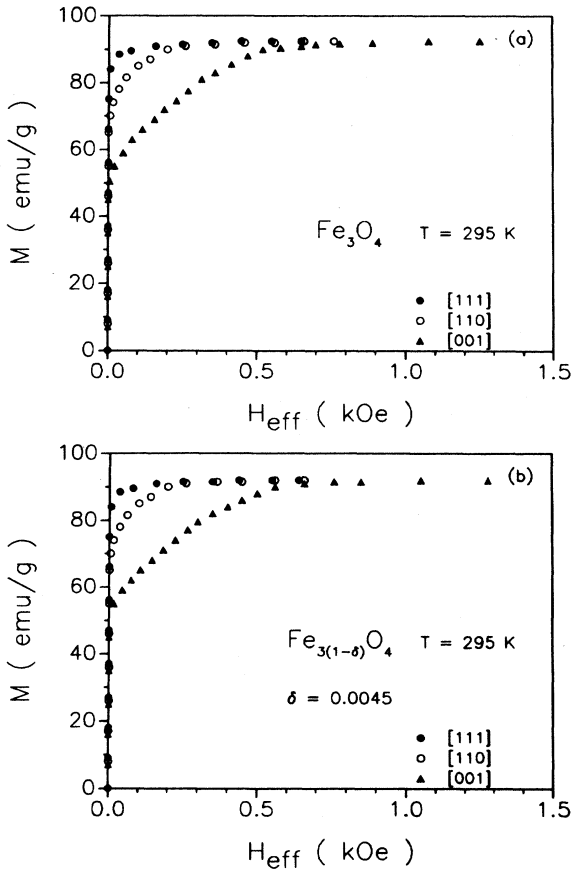

FIG. 1. (a) Magnetization curves of Fe_3O_4 sample for [111], [110], and [001] axes at 295 K. (b) Magnetization curves of $Fe_{3(1-\delta)}O_4$; $\delta=0.0045$ sample for [111], [110], and [001] axes at 295 K.

[$1\bar{1}0$]. Subsequently, samples were cooled in magnetic fields oriented along [001] and measurements carried out in the (010) plane; here both *a-b* and *a-a* twinning occurred. Typical magnetization curves for samples with $\delta=0$ and $\delta=0.0045$ are displayed in Figs. 2(a) and 2(b).

Finally, as an example of the axis-switching effect we exhibit in Fig. 3 a set of magnetization and demagnetization curves for Fe_3O_4 at 105 K, with the magnetic field aligned in the [110] direction (i.e., parallel to the *b* axis). The switching phenomenon is evident in the abrupt changes in the M versus H_{eff} plots.

III. ANALYSIS OF RESULTS

A. Saturation Magnetization

In Fig. 4 the saturation magnetization moments at 4.2 K are shown. Because the oxidation process generates Fe^{3+} ions (as well as cation vacancies) at the expense of Fe^{2+} ions, the saturation moment μ must be a function of δ. The three lines shown in Fig. 4 were calculated on the basis that additional Fe^{3+} ions were created (1) exclusively at octahedral sites, (2) randomly on octahedral and tetrahedral sites, (3) exclusively on tetrahedral sites. One

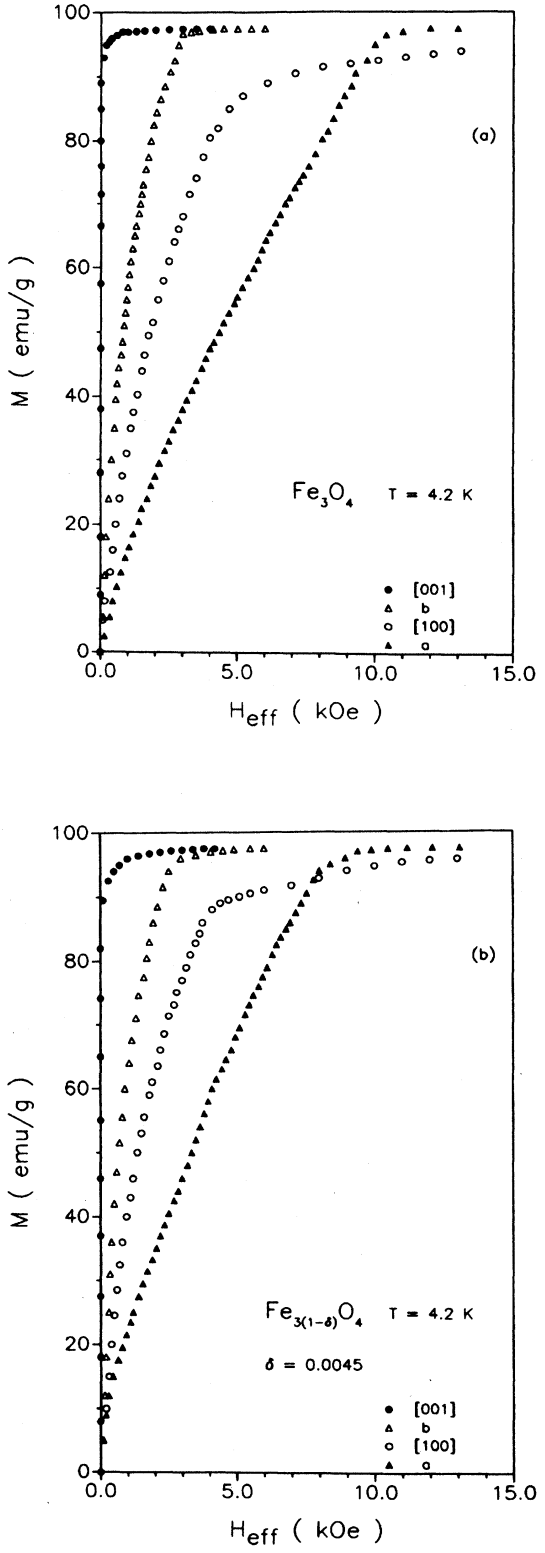

FIG. 2. (a) Magnetization curves of Fe_3O_4 sample for [001], [100], *a* and *b* axes at 4.2 K. (b) Magnetization curves of $Fe_{3(1-\delta)}O_4$; $\delta=0.0045$ sample for [001], [100], *a* and *b* axes at 4.2 K.

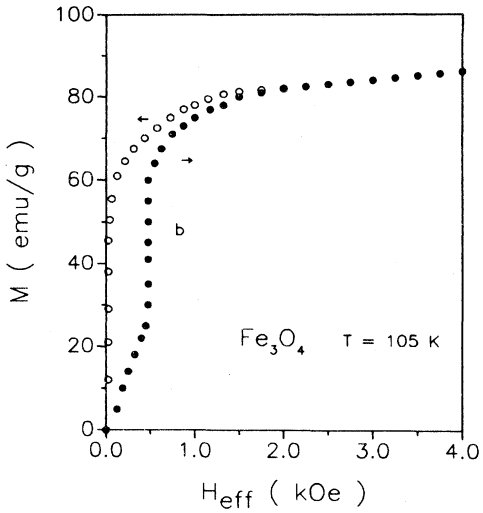

FIG. 3. Magnetization and demagnetization curves of Fe_3O_4 sample along b axis showing axis switching at 105 K.

should note that under the scheme discussed in Sec. I the decrease in magnetic moment per $Fe^{2+} \rightarrow Fe^{3+}$ conversion per monoclinic unit cell in the above three cases would be 0.023, 0.140, and 0.257 Bohr magnetons, respectively.

The experimental points fit extremely well to model (1) as is physically reasonable. This is also in full agreement with data by Ramdani *et al.*[17].

B. Anisotropy energy

The magnetocrystalline anisotropy energy for the cubic phase may be written as[17]

$$E_A = K_1(\alpha_1^2\alpha_2^2+\alpha_2^2\alpha_3^2+\alpha_3^2\alpha_1^2)+K_2\alpha_1^2\alpha_2^2\alpha_3^2+\cdots , \quad (1)$$

where K_1 and K_2 are first- and second-order anisotropy constants and the α_i are the direction cosines with respect to the cubic crystal axes.

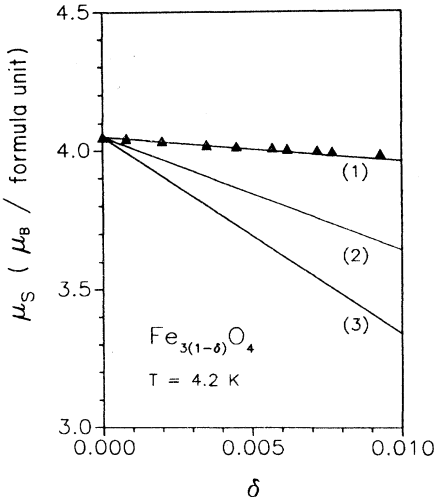

FIG. 4. Saturation moment of $Fe_{3(1-\delta)}O_4$ vs nonstoichiometry δ, at 4.2 K. ▲'s represent experimental data; curves (1), (2), and (3) represent calculated values (explanation in the text).

For the monoclinic phase, in accord with the procedure of Abe *et al.*,[12] we use the following expression:

$$E_A = \mathcal{K}_a\alpha_a^2+\mathcal{K}_b\alpha_b^2+\mathcal{K}_{aa}\alpha_a^4+\mathcal{K}_{bb}\alpha_b^4 +\mathcal{K}_{ab}\alpha_a^2\alpha_b^2-\mathcal{K}_u\alpha_{[\bar{1}11]}^2 , \quad (2)$$

which is the expression employed earlier by Calhoun[10] for an orthorhombic phase, with the last term added to deal with the rhombohedral distortion. Here α_a, α_b, and $\alpha_{[\bar{1}11]}$ are direction cosines with respect to the a, b, and $[\bar{1}11]$ axes of the monoclinic phase, the $\mathcal{K}$'s are corresponding anisotropy constants.

The various $\mathcal{K}$'s were determined either (i) by fitting theoretical curves (1) or (2) to the data, treating the $\mathcal{K}$'s as adjustable parameters, and optimizing the fit by the gradient method; or (ii) by calculating the work required to saturate a given sample. The latter quantity is expressed by

$$W = \int_0^{M_s} H dM \quad (3)$$

and represents the area between the $M(H_{ex})$ curve and the M axis. To allow for internal stresses and the like, one generally calculates only the difference in work W for fields applied along two different directions. As is evident, the areas between the different magnetization curves are very small in Fig. 1 ($T > T_v$), thus leading to considerable error; the areas in Fig. 2 are larger and involve only linear combinations of several $\mathcal{K}$ in Eq. (2). Hence this latter procedure was used only for starting parameters and as a cross check to procedure (i).

C. Calculation of theoretical curves $M(H_{eff})$

It is well established that domain-wall motion in single crystals takes place at very low fields, resulting in saturation of the magnetization along the easy axis direction in quite low fields. The rotation of the magnetization vector against the crystalline anisotropy then becomes a dominant mechanism in the magnetization process. Thus, one calculates magnetization curves (except in the low-field regime) by minimizing the magnetization energy both in the magnetic effective field and in the anisotropy field. The total energy is given by

$$E = E_A - \mathbf{M}_s\cdot\mathbf{H}_{eff}, \quad H_{eff} = H_{ex} - H_D . \quad (4)$$

For $T > T_v$ we let θ represent the angle between the $\mathbf{M}_s$ and the [001] axis, and let ϕ represent the angle between the direction of the M_s projection onto the (001) plane and the [100] axis. Then according to Eq. (1) and (4),

$$E = K_1\sin^2\theta(\sin^2\theta\cos^2\phi\sin^2\phi+\cos^2\theta) +K_2\sin^4\theta\cos^2\theta\sin^2\phi\cos^2\phi -M_sH_{ex}(\alpha_x\sin\theta\cos\phi +\alpha_y\sin\theta\sin\phi+\alpha_z\cos\theta)+NM_s^2 , \quad (5)$$

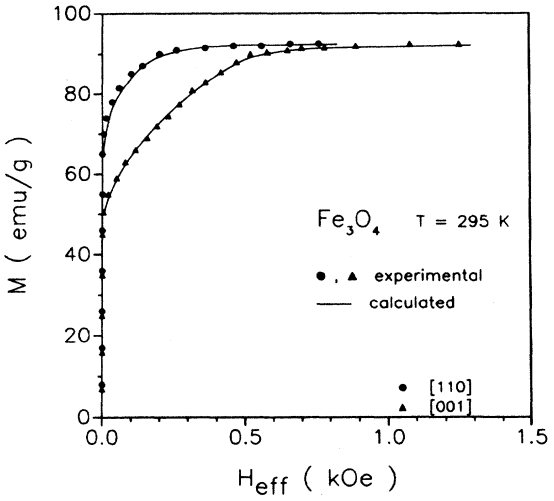

FIG. 5. Calculated magnetization curves of Fe_3O_4 samples at $T=295$ K.

wherein α_x, α_y, and α_z are the direction cosines of the applied field and N is the demagnetization factor. We also introduce the equilibrium constraints

$$\partial E/\partial\theta=\partial E/\partial\phi=0 . \quad (6)$$

The adopted procedure for finding the anisotropy parameters involves the fitting of the theoretical expressions to a particular magnetization curve at a selected temperature, by choosing an initial set of $\mathcal{K}_i(0)$ as input parameters, along with the known $\mathbf{M}_s, N$, and using the conditions (6) to determine θ and ϕ; the latter angles permit one to obtain M. The function $M=M(H)$ is then calculated as a function of H and the resulting curves are compared with the experimental data in the field range where domain-wall motion does not interfere with the analysis.

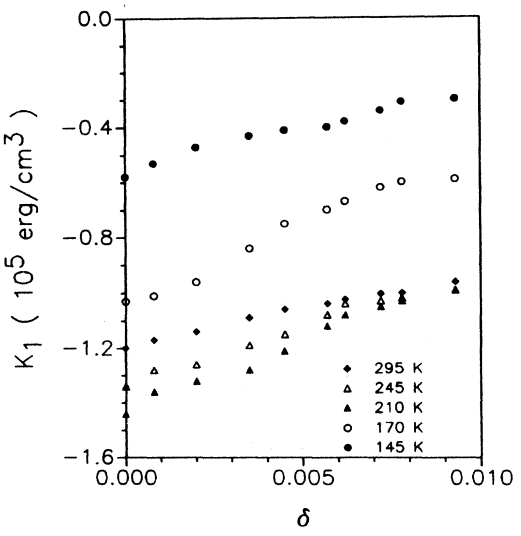

FIG. 6. Anisotropy constant K_1 vs δ for $Fe_{3(1-\delta)}O_4$ in the temperature range 145–295 K.

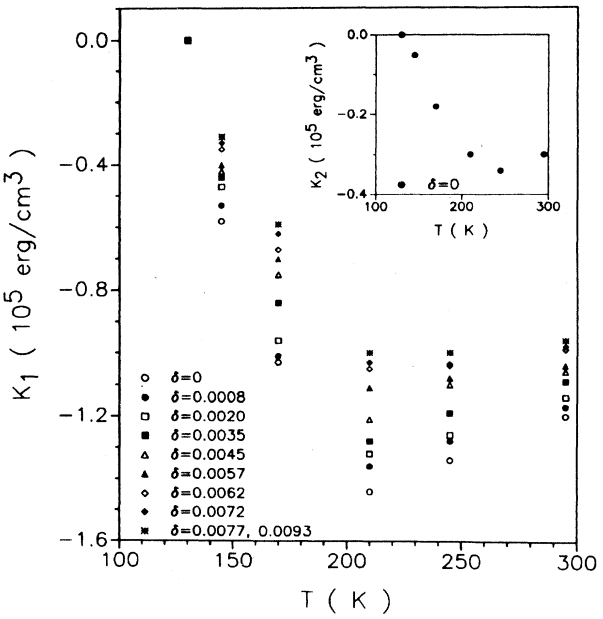

FIG. 7. Temperature dependence of K_1 and K_2 anisotropy parameters for $Fe_{3(1-\delta)}O_4$ series.

A new set $\mathcal{K}_i^{[1]}$ of magnetic anisotropy parameters is then chosen and the procedure repeated to improve the fit; this process is continued until the agreement between theory and experiment is optimized. The preceding steps are then repeated at all other temperatures of interest. Figure 5 shows a comparison of the theoretical with the experimental curve for Fe_3O_4 at $T=295$ K. Comparable fits were achieved for other specimens over a variety of temperatures.

The resulting K_1 values are shown in Fig. 6 as a function of the stoichiometry parameter δ for several temperatures in range 145–295 K; in Fig. 7 is shown the temperature dependence of K_1 for a variety of $Fe_{3(1-\delta)}O_4$ specimens. The insert in Fig. 7 shows the variation of K_2 with T for stoichiometric Fe_3O_4; this curve is nearly the same for all other magnetite specimens under study, independent of δ. The experimental errors for K_1 and K_2 are estimated to be $\pm 5\%$ and $\pm 20\%$, respectively.

The following features are noteworthy. (i) The anisotropy coefficient K_1 vanishes near 130 K for all specimens. This is the isotropy point whose existence has previously been noted.[11,18,19] (ii) K_1 is negative at all temperatures in excess of 130 K and for all δ, and passes through a minimum (maximum anisotropy field) close to 210 K. (iii) As δ increases the $K_1(T)$ dependence becomes less negative and the 210 K minimum becomes more shallow. (iv) There is no discontinuity or other anomaly at the critical value δ_c where the crossover from the first-order to the second-order regime takes place. It should be noted that the present results for stoichiometric magnetite are in good agreement with some earlier work derived both from resonance measurements[11] and from magnetotorque studies.[18,19]

To handle the case $T < T_v$ Eq. (2) was first rewritten in the form

$$E_A = \tilde{\mathcal{K}}_a \alpha_a^2 + \tilde{\mathcal{K}}_b \alpha_b^2 + \mathcal{K}_{aa} \alpha_a^4 + \mathcal{K}_{bb} \alpha_b^4 + \mathcal{K}_{ab} \alpha_a^2 \alpha_b^2 \quad (7)$$

with

$$\tilde{\mathcal{K}}_a \equiv \mathcal{K}_a - \mathcal{K}_u/3 \quad \text{and} \quad \tilde{\mathcal{K}}_b \equiv \mathcal{K}_b + \mathcal{K}_u/3 \, . \quad (8)$$

The expression analogous to Eq. (5) now reads

$$E_A = \tfrac{1}{2}\tilde{\mathcal{K}}_a \sin^2\theta(\cos\phi - \sin\phi)^2 + \tfrac{1}{2}\tilde{\mathcal{K}}_b \sin^2\theta(\cos\phi + \sin\phi)^2 + \tfrac{1}{4}\mathcal{K}_{aa} \sin^4\theta(\cos\phi - \sin\phi)^4 + \tfrac{1}{4}\mathcal{K}_{bb} \sin^4\theta(\cos\phi + \sin\phi)^4 + \tfrac{1}{4}\mathcal{K}_{ab} \sin^4\theta(\cos\phi - \sin\phi)^2(\cos\phi + \sin\phi)^2 - M_x H_{ex}(\alpha_x \sin\theta\cos\phi + \alpha_y \sin\theta \sin\phi + \alpha_z \cos\theta) + N M_s^2 \, . \quad (9)$$

Again, the magnetization curves were calculated after imposing the constraints (6): Using the procedure described earlier, $\tilde{\mathcal{K}}_a$ and $\mathcal{K}_{aa}$ or $\tilde{\mathcal{K}}_b$ and $\mathcal{K}_{bb}$ were found from $M(H_{ex})$ curves measured parallel to the $[1\bar{1}0]$ (a-axis) or the [110] (b-axis) directions. Typical calculated $M(H_{eff})$ curves are compared with the appropriate experimental data in Fig. 8; the agreement is good except at low applied fields where domain-wall motion introduces complications not accounted for by the theory.

The calculation of $\mathcal{K}_{ab}$ is more involved because this requires the determination of the magnetization curve along the [100] direction after the sample has been cooled in a field applied parallel to [001]. Such a procedure establishes the easy axis of magnetization but does not prevent a-b twinning. In these circumstances one cannot calculate the magnetization curves because the magnetization is not a linear superposition of the processes for each separate twin, due to interactions between twinned regions.[10] For further details relating to that problem the reader is referred to Appendix A. (See Fig. 9). Whereas $M(T)$ is a decreasing function of T, $\tilde{K}_b$ increases with T. Thus, additional interactions contribute to the total anisotropy. For example, the Fe^{3+} contribution may not be negligible, or else the mechanism described by Abe *et al.*[12] may be applicable. In the absence of considerably more experimental information it is premature to speculate on the details of these additional interactions.

Thus, $\mathcal{K}_{ab}$ was determined from the area enclosed between the M axis and the $M(H_{ex})$ curve along [100]. It was necessary to extrapolate the $M(H_{ex})$ curves to high fields because the maximum available fields were insufficient to saturate the samples (see Fig. 2). Thus, there is considerable uncertainty in the $\mathcal{K}_{ab}$ values cited below.

The various calculated anisotropy constants are shown in Fig. 10 as plots of $\mathcal{K}$ versus δ at 4.2 K. One should note the strong decrease of $\tilde{\mathcal{K}}_a$ with rising δ and the fact that the remaining parameters have nearly constant values for δ values up to at least 0.007. As $\delta \to 0.012$ all $\mathcal{K} \to 0$.

The temperature variation of the anisotropy parameters is displayed in Figs. 11(a) and 11(b) for specimens with several δ values. The temperature range of measurements is increasingly narrowed with rising δ because of the progressively earlier onset of axis switching. Our

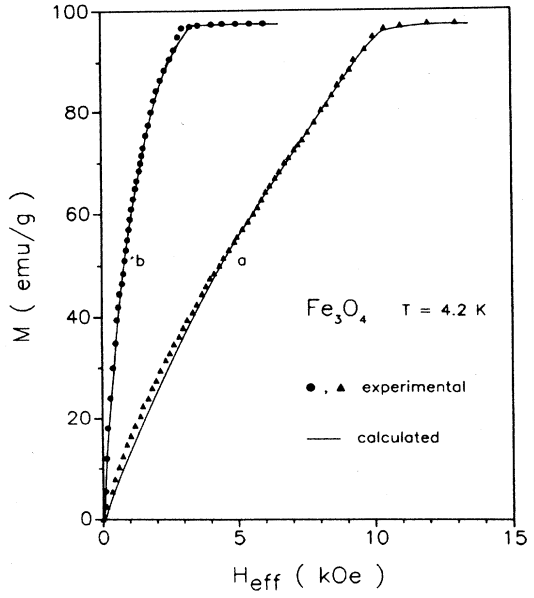

FIG. 8. Calculated magnetization curves of Fe_3O_4 samples at T=4.2 K.

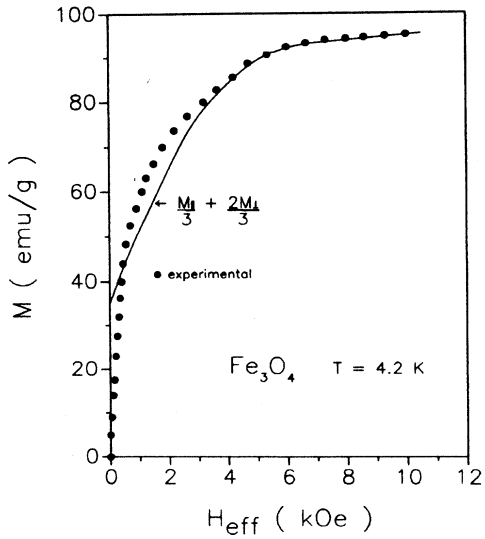

FIG. 9. Magnetization curve of Fe_3O_4 after cooling in zero field. Solid line is calculated under assumption of no interactions.

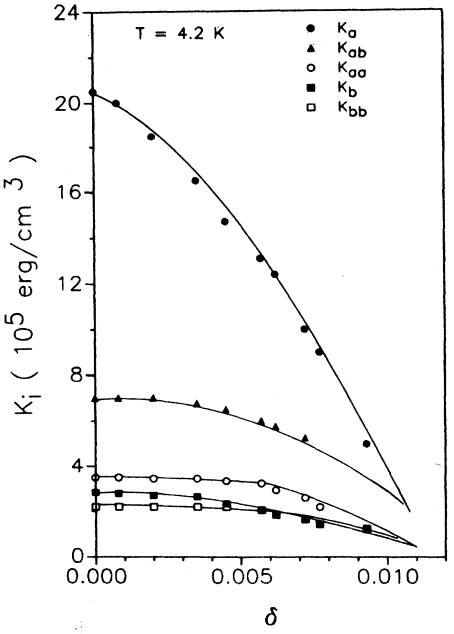

FIG. 10. Anisotropy constants vs δ for $Fe_{3(1-\delta)}O_4$ at 4.2 K.

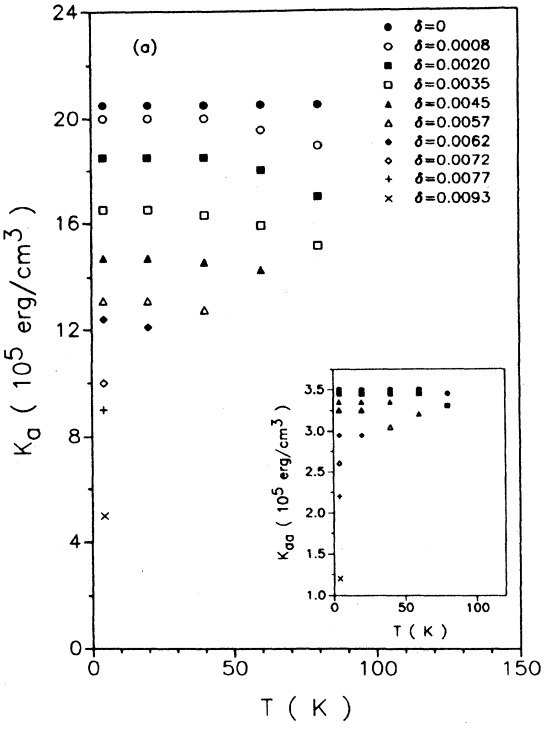

data on stoichiometric magnetite are in excellent agreement with earlier torque measurements by Palmer[20] and differ only slightly from the data reported by Matsui and co-workers.[13] Comparisons with other earlier studies[9,10] is complicated by the fact that incorrect structures were used in the theoretical analysis or because of differences in sample treatment. Note that all $\mathcal{K}$ values are positive and, with the exception of $\tilde{\mathcal{K}}_b$ (which rises with T), not sensitive to temperature changes.

IV. DISCUSSION

These measurements lead to several conclusions.

(1) At a fixed temperature both above and below T_v the various anisotropy parameters vary with δ; this dependence is particularly marked for $\mathcal{K}_a$ and K_1. Of great significance is the fact that a plot of the saturation moment μ versus stoichiometry parameters δ is *linear* (see Fig. 4). If the anisotropy properties were dominated by crystal-field effects one would expect the various $\mathcal{K}$'s to change linearly with δ as well. The single-ion anisotropy is not significantly altered by impurities or lattice vacancies at low concentrations so that neither the average bulk anisotropy symmetry nor the orbital disposition is noticeably changed by small alterations in δ. Thus, if the Fe^{3+} ions are considered magnetically inactive then the decrease in Fe^{2+} concentration should result in a corresponding linear change of anisotropy constants with δ. Since the observed $K(\delta)$ dependences are nonlinear, the single-ion anisotropy cannot be the only factor governing the magnetic properties of magnetite.

(2) A further observation in support of the preceding conclusion is the fact that the temperature variation of

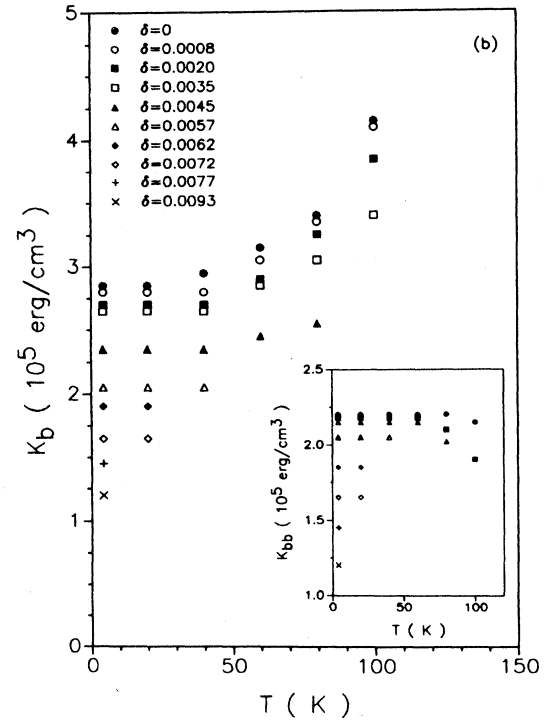

FIG. 11. (a) Temperature dependence of $\tilde{\mathcal{K}}_a$ and $\mathcal{K}_{aa}$ anisotropy parameters for $Fe_{3(1-\delta)}O_4$ series. (b) Temperature dependence of $\tilde{\mathcal{K}}_b$ and $\mathcal{K}_{bb}$ anisotropy parameters for $Fe_{3(1-\delta)}O_4$ series.

$\tilde{\mathcal{K}}_b$ does not follow that of M. If single-ion anisotropy prevailed one would anticipate a relationship of the form[21]

$$k_l(T)/k_l(0) \sim [M(T)/M(0)]^{l(l+1)/2} , \quad (10)$$

where the k_l are the reduced coefficients of the components of the magnetocrystalline anisotropy energy, with the same symmetry as the spherical harmonics $Y_l^m(\theta,\phi)$. Equation (10) would require that $\tilde{\mathcal{K}}_a$ and $\tilde{\mathcal{K}}_b$ vary as the third power in the reduced magnetization $M(T)/M(0)$ and that $\mathcal{K}_{aa}$, $\mathcal{K}_{bb}$, and $\mathcal{K}_{ab}$ vary as the tenth power, contrary to observation.

(3) There is a change in sign of K_1 and K_2 in the range $127 < T_m < 130$ K, which was already noted by earlier investigators. As δ rises T_m diminishes but always remains greater than T_v. This fact indicates that the change in sign of K_1 and K_2 is due to a mechanism unrelated to the Verwey transition. At temperatures between T_m and T_v there is a gradual change in the magnetic structure, possibly an alteration from a ferromagnetic to a conical spin alignment, which affects the magneto-crystalline anisotropy or the magnetostriction. Unfortunately, no magnetostriction measurements have been reported below 120 K, so that this conjecture remains unproven. Alternatively, there is a shift in contributions from different crystal sites to the total anisotropy, roughly along the lines discussed in (1) and (2).

(4) None of the anisotropy parameters shows a shift or slope discontinuity of the critical value δ_c corresponding to the change in the order of the Verwey transition. It is difficult to reconcile this fact with any model in which the Verwey transition is driven primarily by magnetic interactions. This conclusion is reinforced by the fact that the saturation moment changes by less than 0.1% at T_v.[22] Similarly, from neutron scattering, Iizumi *et al.*[6] conclude that the change in magnetic moment across the Verwey transition, due to charge ordering of octahedral cation sites along the monoclinic axis, is at most $0.2\mu_B$.

(5) All $\mathcal{K}$'s approach zero at the extrapolated value $\delta_m \approx 0.012 \approx 3\delta_c$ which also coincides with the highest value of δ for which a transition can still be detected. A more detailed investigation of the change from anisotropic to isotropic magnetic properties is limited by our inability to prepare single-phase magnetite specimens with $\delta > \delta_c$.

(6) $\tilde{\mathcal{K}}_a$ dominates all other contributions to the anisotropy below T_v. This is in consonance with a distortion of the unit cell along the a direction, due to the slight tilting of the c axis from the vertical toward the $-a$ direction of the monoclinic unit cell.

ACKNOWLEDGMENTS

The authors wish to thank Mr. N. Pribble for assistance in the execution of the measurements. This research was supported by National Science Foundation Grant No. DMR 86-16533.

APPENDIX: INTERACTIONS BETWEEN DIFFERENT REGIONS OF A TWINNED SAMPLE

In a study of the mutual torques exerted on each other by the magnetization in neighboring regions Calhoun[10] found the effects to be large. We measured magnetization curves along the [100] direction at 4.2 K after cooling samples with $\delta \leq 0.0072$ in zero field where axis switching presented no problem. If no interactions occurred one would then expect the magnetization curve for $\mathbf{H} \| [100]$ to be given by[10]

$$M_0(H) = \tfrac{1}{3} M_{\|}(H) + \tfrac{2}{3} M_{\perp}(H) , \quad (A1)$$

where $\|$ and $\perp$ refers to magnetization directions parallel and perpendicular to [100]. A comparison of Eq. (A1) with the experiment is furnished in Fig. 9 for stoichiometric magnetite.

While there is a discrepancy between calculated and experimental curves it is smaller than that reported by Calhoun;[10] the difference diminishes with increasing δ. These findings, along with similar results encountered by Rasmussen in electrical transport measurements,[23] suggest that torque interactions between different regions of twinned specimens are relatively weak. However, this does not preclude the existence of other forces that may affect the $M(H)$ curves, such as interactions arising from different types of distortions in neighboring regions.

*Permanent address: Department of Solid State Physics, Akademia Górniczo Hutnicza, 30-059 Kraków, Poland.

[1]E. J. W. Verwey, Nature **144**, 327 (1939); E. J. W. Verwey, P. Haayman, and F. C. Romeijn, J. Chem. Phys. **15**, 181 (1947).
[2]R. Aragón, J. P. Shepherd, J. W. Koenitzer, D. J. Buttrey, R. J. Rasmussen, and J. M. Honig, J. Appl. Phys. **57**, 3221 (1985).
[3]J. P. Shepherd, R. Aragón, J. W. Koenitzer, and J. M. Honig, Phys. Rev. B **32**, 1818 (1985).
[4]R. Aragón, R. J. Rasmussen, J. P. Shepherd, J. W. Koenitzer, and J. M. Honig, J. Magn. Magn. Mater. **54-57**, 1335 (1986).
[5]W. C. Hamilton, Phys. Rev. **110**, 1050 (1958).
[6]M. Iizumi, T. F. Koetzle, G. Shirane, S. Chikazumi, M. Matsui, and S. Todo, Acta. Crystallogr. **38**, 2121 (1982).
[7]L. R. Bickford, Jr., Phys. Rev. **76**, 137 (1949).
[8]C. A. Domenicali, Phys. Rev. **78**, 458 (1950).
[9]H. J. Williams, R. M. Bozorth, and M. Goertz, Phys. Rev. **91**, 1107 (1953).
[10]B. A. Calhoun, Phys. Rev. **94**, 1577 (1954).
[11]S. Chikazumi, in *Magnetism and Magnetic Materials*

(Philadelphia, 1975), Proceedings of the 21st Annual Conference on Magnetism and Magnetic Materials, AIP Conf. Proc. No. 29, edited by J. J. Becker, G. H. Lander, and J. J. Rhyne (AIP, New York, 1976), p. 382.

[12]K. Abe, Y. Miyamoto, and S. Chikazumi, J. Phys. Soc. Jpn. **41**, 1894 (1976), p. 382.

[13]M. Matsui, S. Todo, and S. Chikazumi, J. Phys. Soc. Jpn. **43**, 47 (1977).

[14]H. R. Harrison and R. Aragón, Mater. Res. Bull. **13**, 1097 (1978).

[15]R. Aragón, D. J. Buttrey, J. P. Shepherd, and J. M. Honig, Phys. Rev. B **31**, 430 (1985).

[16]J. P. Shepherd and C. J. Sandberg, Rev. Sci. Instrum. **55**, 1696 (1984).

[17]A. Ramdani, T. Steinmetz, C. Gleitzer, J. M. D. Coey, and J. M. Friedt, J. Phys. Chem. Solids **48**, 217 (1987).

[18]L. R. Bickford, Jr., J. M. Brownlow, and R. F. Penoyer, Proc. Inst. Electr. Eng., Part B **104**, 238 (1957).

[19]Y. Syono and Y. Ishikawa, J. Phys. Soc. Jpn. **18**, 1230 (1963).

[20]W. Palmer, Phys. Rev. **131**, 1057 (1963).

[21]C. Zener, Phys. Rev. **96**, 1335 (1954).

[22]S. Umemura and S. Iida, J. Phys. Soc. Jpn. **40**, 679 (1976).

[23]R. J. Rasmussen, Ph.D. thesis, Purdue University, 1988.